LETTERS

Direct observation of correlations between individual photon emission events of a microcavity laser

J. Wiersig[1]†, C. Gies[1], F. Jahnke[1], M. Aßmann[2], T. Berstermann[2], M. Bayer[2], C. Kistner[3], S. Reitzenstein[3], C. Schneider[3], S. Höfling[3], A. Forchel[3], C. Kruse[1], J. Kalden[1] & D. Hommel[1]

Lasers are recognized for coherent light emission, the onset of which is reflected in a change in the photon statistics[1]. For many years, attempts have been made to directly measure correlations in the individual photon emission events of semiconductor lasers[2,3]. Previously, the temporal decay of these correlations below or at the lasing threshold was considerably faster than could be measured with the time resolution provided by the Hanbury Brown/Twiss measurement set-up[4] used. Here we demonstrate a measurement technique using a streak camera that overcomes this limitation and provides a record of the arrival times of individual photons. This allows us to investigate the dynamical evolution of correlations between the individual photon emission events. We apply our studies to micropillar lasers[5] with semiconductor quantum dots[2,3,6–8] as the active material, operating in the regime of cavity quantum electrodynamics[9]. For laser resonators with a low cavity quality factor, *Q*, a smooth transition from photon bunching to uncorrelated emission with increasing pumping is observed; for high-*Q* resonators, we see a non-monotonic dependence around the threshold where quantum light emission can occur. We identify regimes of dynamical anti-bunching of photons in agreement with the predictions of a microscopic theory that includes semiconductor-specific effects.

Conventional lasers (like gas lasers or semiconductor edge emitters) have a well-defined laser threshold that manifests itself in a sharp increase in the number of emitted photons. Also, the classical and quantum mechanical properties of the emitted light undergo pronounced changes at the laser threshold. The coherence time of the radiation increases strongly and the photon statistics reflects a transition from thermal radiation to coherent emission. The origin of the laser threshold is the loss of the majority of spontaneously emitted photons into non-lasing modes.

Cavity quantum electrodynamics (QED) has opened the door to a new class of lasers that are based on the altered spontaneous-emission properties of the active material, these alterations being due to the modified electromagnetic environment[9]. The Purcell effect makes it possible to inhibit the spontaneous emission into non-lasing modes and enhance that into lasing modes. As a result, in current state-of-the-art semiconductor microcavity lasers[2,3,5–8], the kink in the output intensity as a function of pump rate—previously taken to be a clear indication of a laser threshold—is strongly diminished or even lost.

There are fundamental reasons[10] why the laser threshold is no longer well defined when cavity QED effects become important and the spontaneous emission into non-lasing modes is strongly suppressed. In this regime, the number of photons in the cavity and the number of electronic excitations in the active material are no longer much larger than one, and quantum fluctuations have a central role. Recent advances in the technical realization of semiconductor microcavity lasers have exposed an urgent need for new tools with which to characterize these devices, which operate in a regime that differs fundamentally from that of conventional lasers. This refers both to experimental techniques for characterizing photon correlations and their dynamical evolution on the relevant timescales in semiconductor systems and to quantum statistical models that include semiconductor-specific effects.

The statistical properties of a light beam can be characterized using the second-order, or intensity, autocorrelation function. A classical version of this correlation function was first used by Hanbury Brown and Twiss[4]. Shortly after, Glauber[1] introduced a quantum mechanical description of the second-order correlation function

$$G^{(2)}(t,\tau)=\langle b^{\dagger}(t)b^{\dagger}(t+\tau)b(t+\tau)b(t)\rangle \quad (1)$$

which is often used in its normalized form

$$g^{(2)}(t,\tau)=\frac{G^{(2)}(t,\tau)}{\langle b^{\dagger}(t)b(t)\rangle\langle b^{\dagger}(t+\tau)b(t+\tau)\rangle} \quad (2)$$

Here $b^{\dagger}$ and b are respectively photon creation and annihilation operators of the optical mode of interest, and angle brackets denote the quantum mechanical expectation value with respect to the density operator, ρ.

Under stationary conditions (no t dependence in equations (1) and (2)), the second-order correlation function at zero delay, $\tau = 0$, directly reflects the statistical properties of the emitted light. For conventional lasers with small β factor (describing the fraction of the spontaneous emission into the laser mode relative to the total spontaneous emission), a sharp transition from thermal, $g^{(2)}(0) = 2$, to coherent light emission, $g^{(2)}(0) = 1$, is expected when passing the threshold to lasing. For thermal light, it is also known that $g^{(2)}(\tau)$, as a function of the delay time, decays to unity on the timescale of the coherence time[11]. A drawback of previous investigations of photon correlations in the laser emission was the finite time resolution of the experiments. In a standard Hanbury Brown/Twiss measurement with avalanche photodiodes, the time resolution is about 500 ps, whereas the coherence time of semiconductor lasers below threshold is less than 10 ps (ref. 3). In this example, the experiment averages over a time interval, in which much of the decay of $g^{(2)}(\tau)$ from two to one has taken place. This leads to an underestimation of $g^{(2)}(0)$ and explains the observed below-threshold reduction of the correlation function in previous experiments[2,3].

We consider single-photon sources an important, albeit different, topic because photon anti-bunching is demonstrated in the spontaneous-emission regime of single-atom[12] or single-quantum-dot[13] systems (although the improved time resolution of our new measurement scheme will be beneficial when the Purcell effect is used to shorten the spontaneous lifetime). Earlier experiments on

[1]Physics Department, University of Bremen, 28334 Bremen, Germany. [2]Experimentelle Physik II, Technische Universität Dortmund, 44221 Dortmund, Germany. [3]Technische Physik, University of Würzburg, 97074 Würzburg, Germany. †Present address: Institute for Theoretical Physics, University of Magdeburg, 39016 Magdeburg, Germany.

intensity fluctuations in conventional semiconductor lasers[14] addressed noise in continuous-variable measurements and led to the seminal observation of squeezing as a true quantum effect. Corresponding theoretical investigations based on a Langevin theory were presented, for example, in ref. 15. In this Letter, however, we demonstrate correlations between single-photon events.

For this purpose, we introduce a new measurement scheme that reveals the arrival times of the individual photons in a light beam, thereby allowing us to reconstruct the second-order (and even higher-order) photon correlation functions. The capabilities of this method are demonstrated in the characterization of quantum-dot-based high-Q microcavity lasers. These systems can exhibit a strongly reduced kink in the input and output power traces, as well as the absence of a sharp transition in $g^{(2)}(0)$ between the values reflecting thermal and Poissonian photon statistics, making the threshold no longer well defined. In addition to measurements of $g^{(2)}(\tau = 0)$ without the limitations discussed above, we study the τ dependence of photon correlations and find an unexpected dynamical anti-bunching effect. To verify our results and to address the underlying physics, we use a microscopic theory for photon correlations in the emission of quantum-dot-based microcavity lasers. In the past, the use of single or few quantum-dot emitters for manipulating the photon emission statistics has been suggested, for example in refs 16, 17.

We obtain our experimental results by time-resolved single-photon counting with a resolution down to 2 ps for $g^{(2)}(\tau)$ measurements without the above-discussed limitations. After non-resonant pulsed excitation of the sample, which is held at 6 K, the subsequent emission is recorded with a streak camera in photon counting mode. A fast silicon charge-coupled-device camera is used to read out the streak camera screen. The temporal resolution is achieved by applying high voltage gradients to the horizontal and vertical camera capacitors, causing time-dependent deflections of the photoelectrons inside the streak camera. The camera is synchronized with the exciting laser, such that the sweep period is equal to the laser repetition rate.

Examples of streak camera pictures are shown in Fig. 1. Each dot in Fig. 1b (enlarged for better visibility) corresponds to a single photon detection. For the determination of the second-order correlation function, within each streak the number of photon pairs, the first detected at time t and the second delayed by a time τ, is counted. Normalization is obtained using the product of the average intensities at times t and $t+\tau$ according to equation (2). The resulting normalized correlation function, $g^{(2)}(t,\tau)$, is then averaged over a large number of streaks. Finally, $g^{(2)}(\tau)$ is obtained by averaging over all emission times t. The pictures in Fig. 1 were recorded for a low-Q cavity using III-V semiconductor material.

Extracted results for the second-order photon correlation function, $g^{(2)}(\tau = 0)$, are provided in Fig. 2, together with the corresponding input–output curves, for three different micropillars with cavity qualities Q that increase from Fig. 2a to Fig. 2c. A few characteristic features can be observed. Comparing the input–output curves, the jump from spontaneous to stimulated emission is quite small—about one order of magnitude for the II-VI cavity and two orders of magnitude for the III-V cavities. Furthermore, for the low-Q III-V cavity the jump is rather sharp, whereas for the other two cavities it is smoother. This indicates that the studied samples are strongly influenced by cavity QED effects. From the sample parameters, it may be expected that the low-Q III-V cavity shows the behaviour closest to a conventional laser, as exemplified by the relatively sharp jump in the input–output curve. This jump is already softened for the II-VI cavity, but the variation with cavity parameters suggests that the input–output curve does not provide a unique characterization of the light emission.

Much more insight can be obtained from the zero-delay second-order correlation function. For the II-VI cavity, it shows a transition from values slightly below two (characteristic for thermal light) to those approaching one (suggesting Poisson statistics) in the onset region of stimulated emission. For low excitation, $g^{(2)}(\tau = 0)$ saturates at a value of 1.95, which is less than two as expected for a

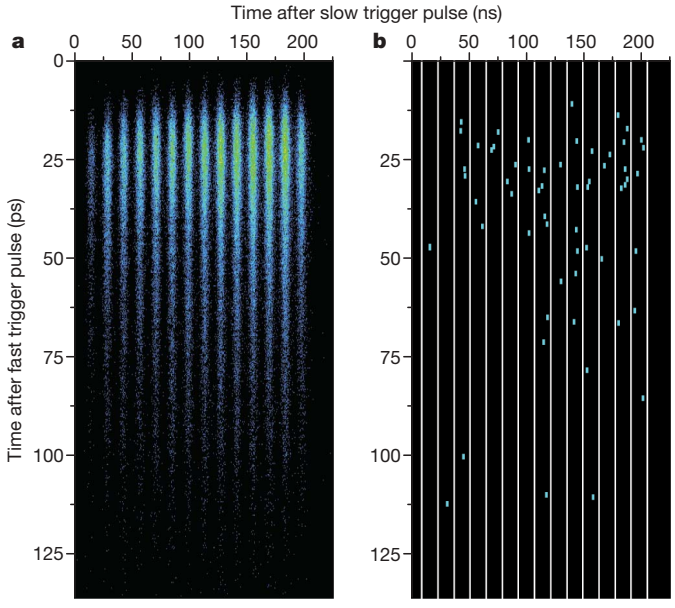

Figure 1 | Time-resolved photon counting statistics. **a**, **b**, Statistics integrated over 60,000 screens (**a**) and for a single screen of the streak camera (**b**), revealing temporal correlations between individual photons. The vertical axes show the temporal resolution after each excitation pulse. Along the horizontal axes the emission after subsequent excitation pulses is displaced. **a** visualizes the statistically averaged emission dynamics after pulsed excitation. For the determination of photon correlations, the signal is read out after only one screen has been filled with a set of streaks, as shown in **b** for 14 excitation pulses. Regions associated with different excitation pulses are separated by lines.

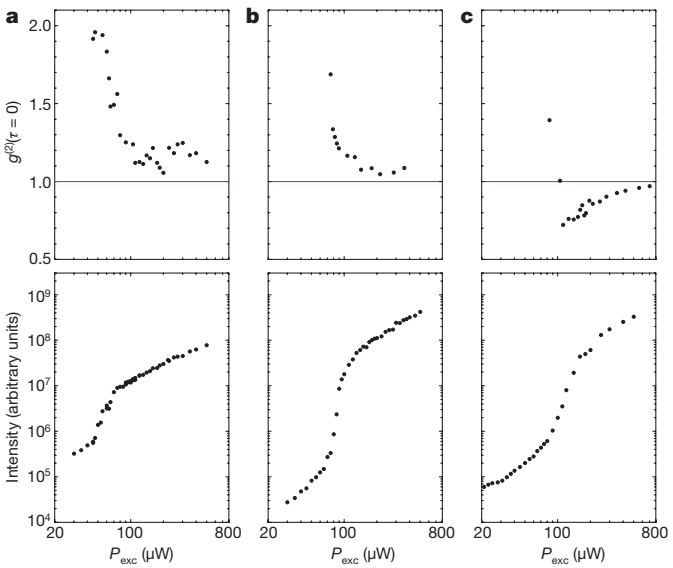

Figure 2 | Measured second-order photon correlation function at zero delay time (top) and output intensity versus input pump power, P_{exc} (bottom), for three different microcavity lasers. **a**, The II-VI cavity, which has a diameter of 1.5 μm, has a low Q factor, of 1,850, for the lowest confined photon mode. Twenty quantum dots were estimated, from the quantum-dot density and the spectral overlap of their emission with the optical mode, to be involved. **b**, **c**, For the III-V cavities of diameters 5 μm (**b**) and 8 μm (**c**), Q factors of 9,000 and 19,000 and effective quantum-dot numbers of 30 and 15 were estimated, respectively.

conventional (low-β) laser. As the power is increased, a smooth drop towards unity is seen as the lasing threshold region is passed. The low-Q III-V cavity shows a similar dependence. For the high-Q III-V cavity, however, $g^{(2)}(\tau = 0)$ unexpectedly drops to values below unity around the lasing threshold, giving clear evidence for the emission of non-classical light. This is accompanied by an even smoother input–output curve. For the III-V cavities, the correlations could not be measured well below the threshold region owing to the limited sensitivity of the streak camera for wavelengths above 900 nm.

Our experimental set-up also provides access to the second-order correlation function at finite delay times. This allows us to study the dynamical evolution of the photon correlations in semiconductor microlasers. In Fig. 3, we display the evolution of the correlations for the III-V cavities and three different excitation powers. For the low-Q cavity (Fig. 3a) and excitation below the threshold region, $g^{(2)}(\tau)$ drops smoothly from a value slightly below two towards unity within the first picoseconds. However, for delays of around 40 ps, values below unity appear. The data for the II-VI cavity are similar to those for the low-Q cavity. For the high-Q cavity (Fig. 3b) and excitation in the threshold region, pronounced long-lasting oscillations of $g^{(2)}(\tau)$ are visible. To ensure that this effect is not caused by noise or lack of statistics, we studied the power dependence of the amplitude and frequency of the oscillations and found systematic variations (not shown). The oscillations become obviously damped with increasing excitation power. Above threshold, we find that $g^{(2)}(\tau) \approx 1$ in both the low-Q case and the high-Q case.

For $g^{(2)}(0)$, a semiconductor theory has been developed recently[18] using the cluster expansion technique[19–21]. In contrast to models based on atomic systems, this theory is capable of incorporating semiconductor-specific features such as Pauli blocking, Coulomb interaction and a modified source term for spontaneous emission[22–24]. The starting point of the microscopic theory is a semiconductor Hamiltonian for the interacting carrier–photon system. The time evolution of the photon number in the laser mode, $\langle b^\dagger b\rangle$, and the electron, $f_\nu^{\mathrm{e}} = \langle c_\nu^\dagger c_\nu\rangle$, and hole, $f_\nu^{\mathrm{h}} = 1 - \langle v_\nu^\dagger v_\nu\rangle$, populations is determined by using Heisenberg's equations of motion. Here $c_\nu^\dagger$ and c_ν and $v_\nu^\dagger$ and v_ν are the creation and annihilation operators of electrons in the conduction and, respectively, valence band states ν. Cavity losses are introduced by coupling the system to an external reservoir. Scattering and dephasing are treated in the relaxation-time approximation.

Here we extend the theory to finite delay times, τ. Suppressing the dependence on t, we rewrite equation (1) as

$$G^{(2)}(\tau) = \langle\langle b^\dagger(\tau) b(\tau)\rangle\rangle \langle b^\dagger b\rangle$$

where the expectation value $\langle\langle \cdots \rangle\rangle$ is taken with respect to the modified density operator $\tilde{\rho} = b\rho b^\dagger / \langle b^\dagger b\rangle$. This way, we reduce the two-time problem to two single-time problems that can be solved successively. Our approach, which is applied to the nonlinear equations of motion describing semiconductor systems, becomes the quantum regression theorem[25] for linear systems of equations, as frequently used for two-level systems.

In Fig. 4, we show examples of the numerical calculations. They are intended to demonstrate possible results for two different sets of parameters. The data are sensitive to the microscopic description of the carrier scattering that provides a common source for carrier redistribution and dephasing. These processes depend on, among other things, the electronic states—both for the recombination processes and for where the carriers are pumped. To simplify this rather involved analysis, we assume pumping at higher quantum-dot states; for a more direct comparison with the experiments, excitation of delocalized barrier states and subsequent capture and relaxation processes should be considered. We attribute deviations (such as the stronger damping of the oscillations in Fig. 4d) to the simplifications in the quantum-dot model. Nevertheless, the chosen examples reproduce the general trends of the experiments.

The value of $g^{(2)}(0)$ calculated for the low-Q case does not reach the subthreshold value of two for thermal light, in agreement with experiment. This has been identified before as a characteristic of microcavity lasers with larger β factors and a small numbers of emitters[3]. The corresponding calculations of $g^{(2)}(\tau)$ for low excitation intensities show a non-monotonic decay to unity from the initial value, $g^{(2)}(0)$. In the higher-Q case, we find an anti-bunching effect ($g^{(2)}(0) < 1$ and oscillations in $g^{(2)}(\tau)$), as seen in the experimental data.

The observed oscillations in the photon correlations are a result of the dynamical coupling between photons and carriers and can be qualitatively understood as follows. For a microcavity operated at steady state in the spontaneous-emission regime, $g^{(2)}(\tau)$ decays from (nearly) two to one on the timescale of the coherence time. In the regime of dominating stimulated emission, $g^{(2)}(\tau)$ equals one independently of time delay. The oscillations are observed in the regime of transition from spontaneous to stimulated emission in a system that, under these conditions, contains only very few photons emitted by very few quantum dots. This is the transition regime of cavity QED lasers discussed in ref. 10. Unlike in the situation in the lasing regime, here the loss of a photon from of the cavity represents a severe perturbation of the system, which strongly influences the coupled carrier–photon dynamics.

Systems of emitters coupled to a cavity mode are known to exhibit different kinds of oscillations of the emission intensity. Relaxation oscillations can occur close to the threshold region when the laser is switched on or perturbed, and Rabi oscillations can occur in the

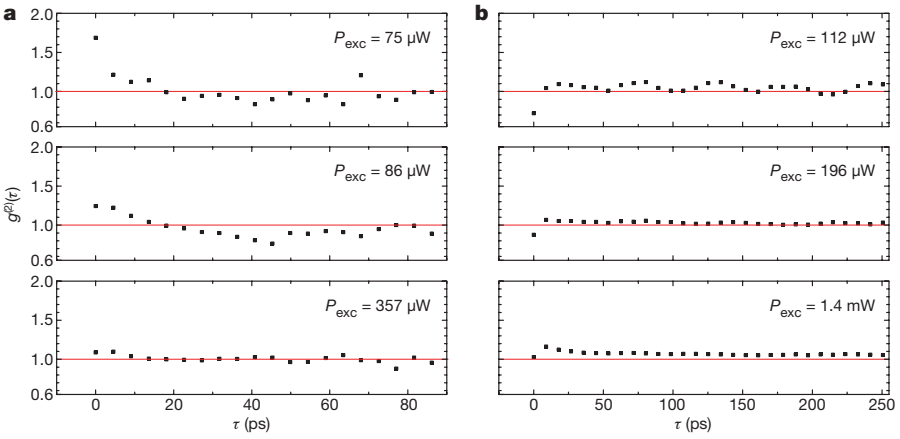

Figure 3 | Measured temporal evolution of the second-order correlation function for selected pump powers, P_{exc}. Results for the III-V cavities of Fig. 2: **a**, low-Q micropillar; **b**, high-Q micropillar. An unexpected outcome is the appearance of dynamical anti-bunching ($g^{(2)}(\tau) < 1$) for low and intermediate excitation densities at finite τ for the low-Q cavity. The intensity correlation function does not merely drop to a value of unity, but takes on smaller values with subsequent oscillations; this is particularly clear for the high-Q cavity with $P = 112$ μW.

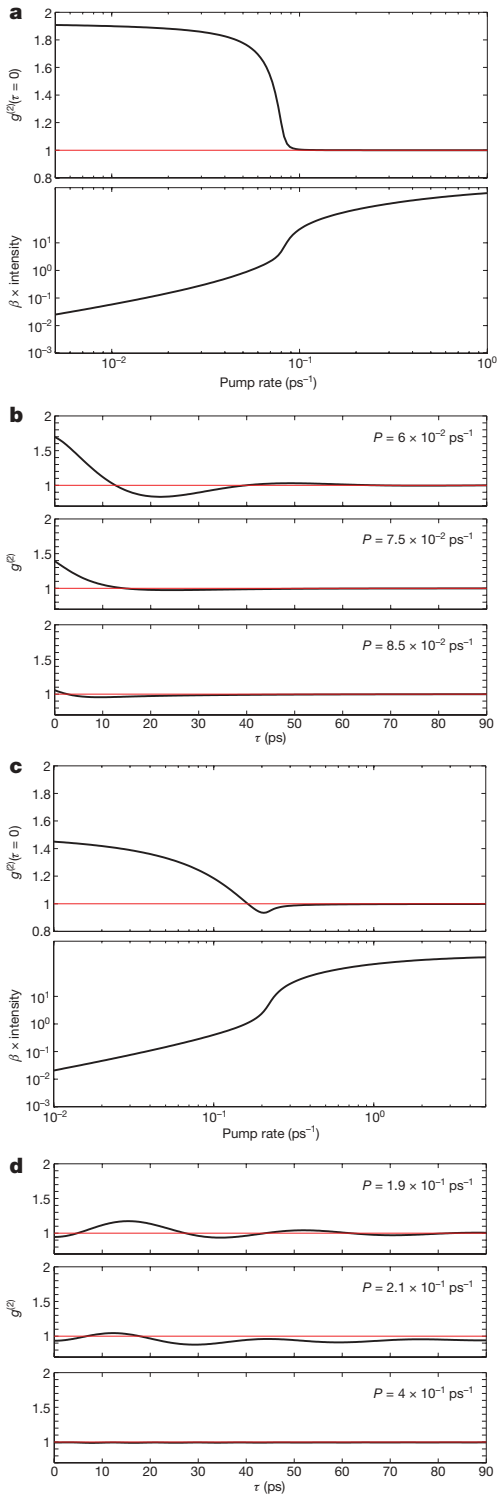

Figure 4 | Calculated zero-delay correlation functions, input–output curves and temporal dynamics of $g^{(2)}(\tau)$. a, **b**, Low-Q quantum-dot microcavity laser; **c**, **d**, high-Q quantum-dot microcavity laser. Selected pump rates, P, are used in **b** and **d**.

regime in which the dissipation is small in comparison with the light–matter coupling strength. The dynamics of the correlation function $g^{(2)}(\tau)$ can be traced back to this behaviour. Our theory predicts that both kinds of oscillations can be triggered by photon emission events. In reaction to the perturbation, the system tries to re-establish equilibrium, and, in doing so, undergoes quantum oscillations. In both cases, the origin of these oscillations is the feedback due to the cavity, which can lead to out-of-phase oscillations of photon number and lasing medium. These oscillations become damped as the pump rate increases and a regime of stimulated emission is reached in which the photon number is high enough that single photon losses no longer affect the system considerably.

In our case, the perturbation of the few-emitter system can become so prominent that, for example, the subsequent emission of a photon is suppressed. This leads to the dynamic anti-bunching both for zero delay and for times after enhanced photon pair emission during the oscillations.

These oscillations potentially also appear in intensity measurements. However, as the moment of photon emission is stochastic, any time averaging blurs the oscillations. Nevertheless, the oscillations also carry over to the correlation functions similar to $g^{(2)}(\tau)$. There they survive the averaging, as although the moment of arrival of the first photon is still stochastic, a second photon is picked whose delay, τ, relative to the first is fixed for all detected photon pairs. For increasing Q, the cavity feedback is enhanced, causing the quantum fluctuations to become more pronounced as reflected by the oscillations of $g^{(2)}(\tau)$.

In conclusion, we have presented a new measurement scheme with the necessary time resolution to fully access photon correlations on a single-photon level, yielding a record of arrival times of individual photons. From these data, correlation functions can be constructed to arbitrary order, facilitating a complete characterization of the light source. Our approach can be viewed as the most direct experimental realization of the pioneering theory in ref. 1. To give an example of these possibilities, we show results for the third-order correlation function in Fig. 5. Higher-order correlations in the light emission may provide a detailed understanding of the nature of quantum many-particle states such as those currently discussed for microcavities in the regime of strong light–matter coupling.

The validity of the reported results is not restricted to semiconductor micropillars: similar results are expected for all light sources that involve a small number of emitters, be they atoms, molecules, defects in solids or semiconductor quantum structures. We expect our findings and methods to mark the starting point for novel quantum optical studies addressing the dynamics of correlation functions of light.

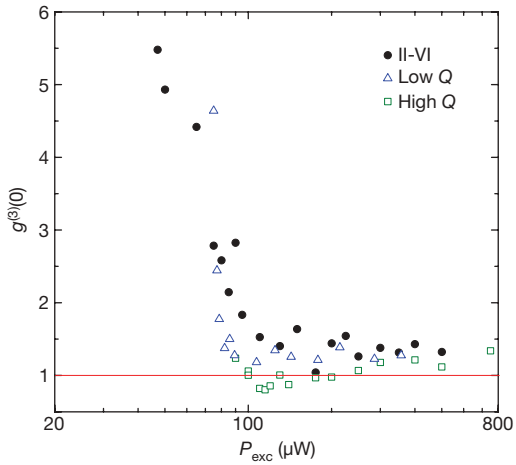

Figure 5 | Measured third-order correlation function $g^{(3)}(0)$. Characterization of the simultaneous arrival of three photons as a function of excitation power, for the three different micropillar samples studied in this paper. For the II-VI and low-Q resonators, the time resolution was increased to about 20 ps. These two samples show values close to the theoretical prediction, $g^{(3)}(0) = 6$, at lowest excitation powers. The kth-order correlation functions for a thermal source of radiation are readily obtained from the factorial moments of the Planck distribution, $\langle n(n-1)\cdots(n-k+1)\rangle = k!\langle n\rangle^k$, to give $g^{(k)}(0) = k!$, corresponding to the number of permutations of indistinguishable photons.

METHODS SUMMARY

Experimental set-up. For the intensity correlation measurements, we used a microscope objective to focus and collect the light. An interference filter with a bandwidth of 1 nm singled out the fundamental-mode emission of the microcavity. The normalized correlation function, $g^{(2)}(t,\tau)$, was determined by dividing the number of photon pairs detected using the streak camera at times t and $t+\tau$ by the product of the mean photon counting rates at the same times. Weighted averaging over all times t gave $g^{(2)}(\tau)$. To exclude noise or saturation effects, correlation measurements were also performed on a pulsed laser with several levels of attenuation, showing no deviations from the expected value, $g^{(2)}(0)=1$.

Full Methods and any associated references are available in the online version of the paper at www.nature.com/nature.

Received 12 January; accepted 28 April 2009.

1. Glauber, R. J. The quantum theory of optical coherence. *Phys. Rev.* **130,** 2529–2539 (1963).
2. Strauf, S. *et al.* Self-tuned quantum dot gain in photonic crystal lasers. *Phys. Rev. Lett.* **96,** 127404 (2006).
3. Ulrich, S. M. *et al.* Photon statistics of semiconductor microcavity lasers. *Phys. Rev. Lett.* **98,** 043906 (2007).
4. Hanbury Brown, R. & Twiss, R. Q. Correlation between photons in two coherent beams of light. *Nature* **177,** 27–29 (1956).
5. Vahala, K. J. Optical microcavities. *Nature* **424,** 839–846 (2003).
6. Choi, J.-S. *et al.* Evolution of the onset of coherence in a family of photonic crystal nanolasers. *Appl. Phys. Lett.* **91,** 031108 (2007).
7. Xie, Z. G., Götzinger, S., Fang, W., Cao, H. & Solomon, G. S. Influence of a single quantum dot state on the characteristics of a microdisk laser. *Phys. Rev. Lett.* **98,** 117401 (2007).
8. Reitzenstein, S. *et al.* Single quantum dot controlled lasing effects in high-*Q* micropillar cavities. *Opt. Express* **16,** 4848–4857 (2008).
9. Berman, P. *Cavity Quantum Electrodynamics* (Academic, 1994).
10. Rice, P. R. & Carmichael, H. J. Photon statistics of a cavity QED laser: a comment on the laser-phase-transition analogy. *Phys. Rev. A* **50,** 4318–4329 (1994).
11. Loudon, R. *The Quantum Theory of Light* 2nd edn (Clarendon, 1983).
12. Kimble, H. J., Dagenais, M. & Mandel, L. Photon antibunching in resonance fluorescence. *Phys. Rev. Lett.* **39,** 691–695 (1977).
13. Michler, P. *et al.* A quantum dot single-photon turnstile device. *Science* **290,** 2282–2285 (2000).
14. Machida, S., Yamamoto, Y. & Itaya, Y. Observation of amplitude squeezing in a constant-current-driven semiconductor laser. *Phys. Rev. Lett.* **58,** 1000–1003 (1987).
15. Hofmann, H. F. & Hess, O. Coexistence of thermal noise and squeezing in the intensity fluctuations of small laser diodes. *J. Opt. Soc. Am. B* **17,** 1926–1933 (2000).
16. Wiele, C., Haake, F., Rocke, C. & Wixforth, A. Photon trains and lasing: the periodically pumped quantum dot. *Phys. Rev. A* **58,** R2680–R2683 (1998).
17. Benson, O. & Yamamoto, Y. Master-equation model of a single-quantum-dot microsphere laser. *Phys. Rev. A* **59,** 4756–4763 (1999).
18. Gies, C., Wiersig, J., Lorke, M. & Jahnke, F. Semiconductor model for quantum dot-based microcavity lasers. *Phys. Rev. A* **75,** 013803 (2007).
19. Fricke, J. Transport equations including many-particle correlations for an arbitrary quantum system: a general formalism. *Ann. Phys.* **252,** 479–498 (1996).
20. Hoyer, W., Kira, M. & Koch, S. W. in *Nonequilibrium Physics at Short Time Scales* (ed. Morawetz, K.) 309–338 (Springer, 2004).
21. Kira, M., Jahnke, F., Hoyer, W. & Koch, S. W. Quantum theory of spontaneous emission and coherent effects in semiconductor microstructures. *Prog. Quantum Electron.* **23,** 189–279 (1999).
22. Schwab, M. *et al.* Radiative emission dynamics of quantum dots in a single cavity micropillar. *Phys. Rev. B* **74,** 045323 (2006).
23. Baer, N., Gies, C., Wiersig, J. & Jahnke, F. Luminescence of a semiconductor quantum dot system. *Eur. Phys. J. B* **50,** 411–418 (2006).
24. Berstermann, T. *et al.* Systematic study of carrier correlations in the electron-hole recombination dynamics of quantum dots. *Phys. Rev. B* **76,** 165318 (2007).
25. Carmichael, H. J. *Statistical Methods in Quantum Optics 1* (Springer, 1998).

Supplementary Information is linked to the online version of the paper at www.nature.com/nature.

Acknowledgements We would like to thank P. Gartner and I. Akimov for discussions and technical support. Funding from the Deutsche Forschungsgemeinschaft through the research group 'Quantum optics in semiconductor nanostructures' and a grant for CPU time at the Forschungszentrum Jülich (Germany) is gratefully acknowledged.

Author Contributions Experiments were performed in Dortmund by M.A., T.B. and M.B., with the participation of C. Kistner. Calculations were done in Bremen by J.W., C.G. and F.J. The III-V samples were grown in Würzburg by C. Kistner, S.R., C.S., S.H. and A.F. The II-VI sample was prepared in Bremen by C. Kruse, J.K. and D.H.

Author Information Reprints and permissions information is available at www.nature.com/reprints. Correspondence and requests for materials should be addressed to F.J. (jahnke@itp.uni-bremen.de) or M.B. (manfred.bayer@tu-dortmund.de).

METHODS

Sample preparation. The cylindrical low-Q and high-Q III-V micropillar samples were grown by molecular beam epitaxy on a GaAs substrate. The distributed Bragg reflectors consisted of 20 upper and 23 lower alternating layers of AlAs (79 nm)–GaAs (67 nm) $\lambda/4$ pairs for the low-Q micropillar and 26 upper and 33 lower alternating layers of AlAs (74 nm)–GaAs (68 nm) $\lambda/4$ pairs for the high-Q micropillar. The central λ cavity contained one layer of self-assembled InGaAs quantum dots with a density of $\sim 3 \times 10^{10}\,\mathrm{cm}^{-2}$ in the low-Q case and one layer of self-assembled AlGaInAs quantum dots with a density of $\sim 6 \times 10^{9}\,\mathrm{cm}^{-2}$ in the high-Q case, from which cavities with diameters of several micrometres were fabricated by means of high-resolution electron beam lithography and plasma-induced reactive ion etching.

The II-VI sample was also grown by molecular beam epitaxy. There the distributed Bragg reflectors consisted of 15 upper and 18 bottom layers in which $ZnS_{0.06}Se_{0.94}$ (48 nm) layers were used as high-index material and a 25.5-period MgS (1.7 nm)–ZnCdSe (0.6 nm) superlattice was used as low-index material. The central λ cavity contained a single sheet of CdSe/ZnSe quantum dots with an approximate density of $\sim 5 \times 10^{10}\,\mathrm{cm}^{-2}$.

To estimate the number of quantum dots involved in the light emission, we multiplied the dot density of the as-grown sample by the effective photon mode area in the pillar plane. Then we scaled this number by the spectral overlap between the inhomogeneous dot emission and the width of the mode in the lasing regime. Below threshold, the spectral width of the mode is larger, but simultaneously fewer quantum dots are excited by the laser. Therefore, for simplicity we used the same number of quantum dots over the whole excitation power range.

Experimental set-up. The sample was mounted in a helium-flow microscopy cryostat, in which temperatures as low as 6 K could be achieved. A Ti:sapphire laser operating at $\lambda = 780$ nm with pulse durations of $\sim$100 fs and a repetition frequency of 76 MHz was used for excitation, corresponding to 13.2-ns pulse separation. A microscope objective with a focal length of 2 cm and a numerical aperture of 0.26 was used to focus and collect the light. After collection, the emission was directed into the streak camera. An interference filter with a bandwidth of 1 nm was used to single out the fundamental-mode emission of the microcavity. To ensure that the measured correlations did not arise as a result of noise in the charge-coupled device or saturation effects, we performed additional correlation measurements on an attenuated pulsed laser. We varied the pulsed laser intensity over the whole range of intensities used in this paper, but no deviations from the expected result ($g^{(2)}(0) = 1$) were found.

Obtaining $g^{(2)}$ from experimental data. The normalized correlation function, $g^{(2)}(t, \tau)$, is the number of photon pairs detected at times t and $t + \tau$ divided by the number of photon pairs that would be detected if the photons had the same temporal intensity profile but were emitted statistically independently of each other. The number of detected photon pairs is thus directly available in the recorded single screens of the streak camera. This number is equivalent to the non-normalized correlation function, $G^{(2)}(t, \tau)$, which is usually measured using a Hanbury Brown/Twiss set-up. In the case of statistically independent photons, the information about the number of expected photon pairs is completely determined by the mean intensities at times t and $t + \tau$. Therefore, the normalization of $g^{(2)}(t, t + \tau)$ can be calculated from the intensity profile integrated over all screens. Summing all photon pairs at various times, t, and for a fixed delay, τ, and dividing this number by the sum of the expected statistically independent photon pairs for variable t values and fixed τ, gives the time-averaged function $g^{(2)}(\tau)$. In the excitation density regime of the transition from spontaneous to stimulated emission, and above, the photon pairs at late t (when the emission is purely spontaneous) have a negligible influence on the photon statistics.

Quantum-dot parameters. In the numerical calculations, we assumed that 50 quantum dots in the low-Q micropillar and eight quantum dots in the high-Q micropillar were resonant with the optical mode. We chose a spontaneous-emission factor of $\beta = 0.1$, a total spontaneous-emission time (enhanced as a result of the Purcell effect) of $\tau_{sp} = 1.7$ ps (low Q) or 0.75 ps (high Q), and a quality factor of $Q = 40{,}000$ (low) or 80,000 (high). We note that the experimental Q factors are lower bounds, as they are determined for weak excitation below the transparency point. Considering resonant pumping of carriers in the quantum-dot p shell, we used a relaxation time from p shell to s shell of 0.5 ps for electrons and 0.25 ps for holes. Further details of the quantum-dot model are given in ref. 23.

Details of calculations. Coupled equations of motion for various expectation values and correlation functions can be obtained[18] using Heisenberg's equations of motion for the carrier and photon operators. To truncate the arising hierarchy of equations, the cluster expansion method[19,20] was used. In this approach, operator averages are classified into singlets, doublets, triplets, quadruplets, etc., according to the number of particles they involve. Mixed expectation values with carrier and photon operators are classified accordingly, keeping in mind that a photon operator is linked to two carrier operators[21]. Truncation on the doublet level has been used to describe photoluminescence from quantum dots[23]. To compute the photon statistics in terms of $g^{(2)}(0)$, truncation at the quadruplet level is required[18].

First we computed $\langle b^\dagger(t)b(t)\rangle$, $\langle b^\dagger(t)b^\dagger(t)b(t)b(t)\rangle$, $\langle b^\dagger(t)b(t)c^\dagger(t)c(t)\rangle$, … with $t \to \infty$ according to the single-time equations of motion on quadruplet level as discussed in ref. 18. In a second step, the τ dynamics of

$$G^{(2)}(\tau) = \langle\langle b^\dagger(\tau)b(\tau)\rangle\rangle\langle b^\dagger b\rangle$$

was evaluated using the single-time equations of motion for $\langle\langle b^\dagger(\tau)b(\tau)\rangle\rangle$, $\langle\langle c_v^\dagger(\tau)c_v(\tau)\rangle\rangle$, … with the initial conditions

$$\langle\langle b^\dagger(\tau)b(\tau)\rangle\rangle|_{\tau=0} = \langle b^\dagger b^\dagger bb\rangle/\langle b^\dagger b\rangle$$

$$\langle\langle c_v^\dagger(\tau)c_v(\tau)\rangle\rangle|_{\tau=0} = \langle b^\dagger bc_v^\dagger c_v\rangle/\langle b^\dagger b\rangle$$

and so on. The underlying assumption is that the truncation introduced by the cluster expansion works equally well for operator averages taken with respect to the density operators ρ and $\tilde{\rho}$.